Supporting Information

Purposely Designed Hierarchical Porous Electrodes for High Rate Microbial Electrosynthesis of Acetate from Carbon Dioxide

Victoria Flexer[1,*] and Ludovic Jourdin[2]

[1] Centro de Investigación y Desarrollo en Materiales Avanzados y Almacenamiento de Energía de Jujuy-CIDMEJu (CONICET-Universidad Nacional de Jujuy). Av. Martijena S/N, Palpalá, 4612, Argentina.

[2] Department of Biotechnology, Delft University of Technology, Van der Maasweg 9, 2629 HZ Delft, The Netherlands.

*Corresponding author: vflexer@unju.edu.ar

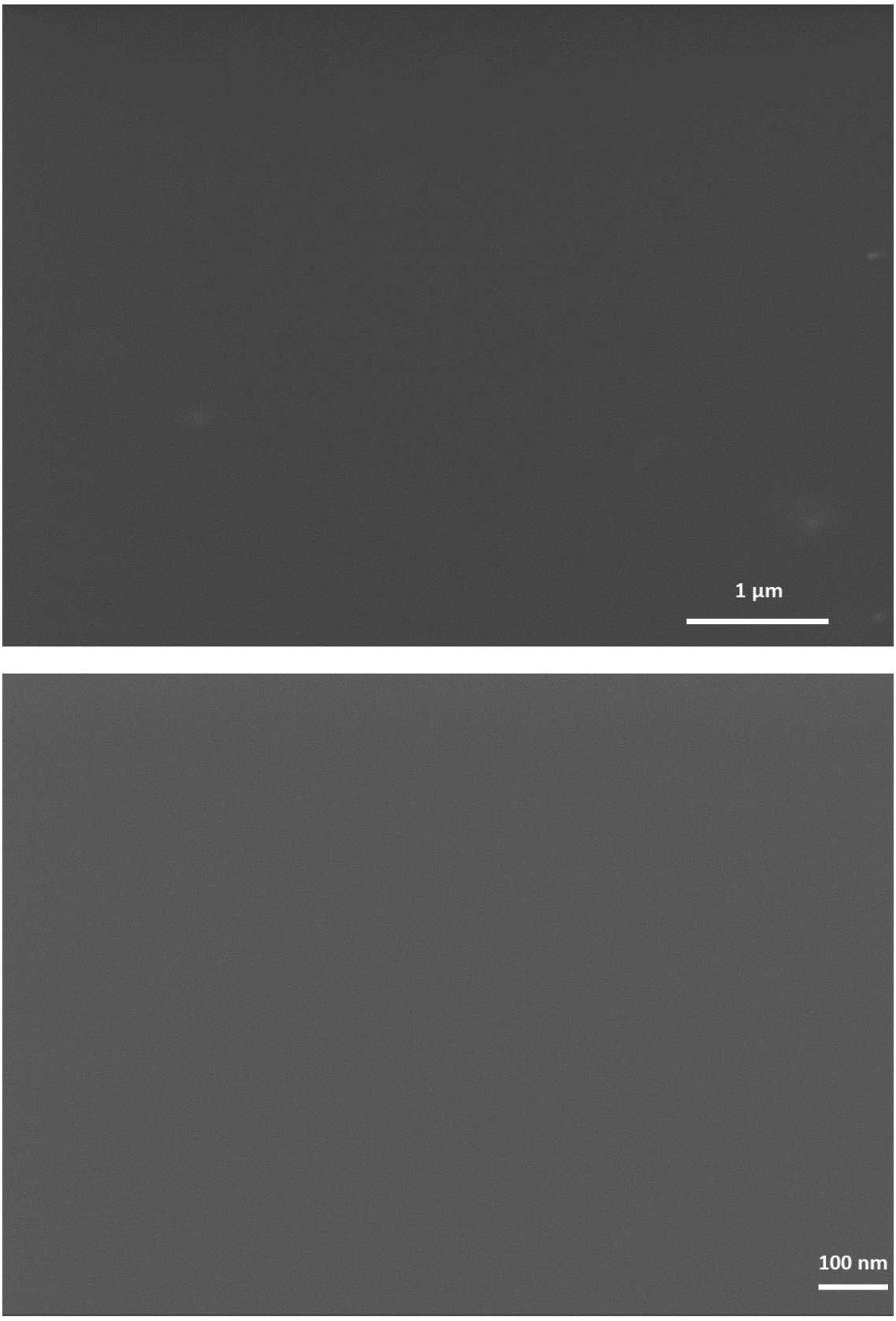

Figure S1: SEM micrographs for RVC at different magnification. The images show extremely flat surfaces, with no remarkable features. Both images are almost one single shade of grey, since they correspond to almost atomically flat surfaces. These images are in clear contrast with both EPD-3D and NanoWeb-RVC (figures 2 H, L and M, at the same scales in the main text).

Experimental details for the Bioelectrochemical Experiments

Source of microorganisms

Experiments on NanoWeb-RVC:
A mixed microbial consortium from natural environments (stormwater pond sediments, located on the University of Queensland, St Lucia campus, Brisbane, Australia) and engineered anaerobic systems (from the Luggage Point Waste Water Treatment Plant anaerobic digester, Brisbane, Australia) were combined and added to a final concentration of 60 $mg_{COD}.L^{-1}$ in the reactors on the same day.

Experiments on EPD-3D:
Planktonic cells from the microbial electrosynthesis systems using NanoWeb-RVC (reference 27 in the main manuscript) after half a year of operation were collected, centrifuged, resuspended in fresh catholyte, and used as inoculum for the MESs. Therefore, no organics were introduced in the new reactors. The enriched inoculum was added to a final concentration of about 200 mg L^{-1} as the chemical oxygen demand (COD) in each reactor.

Electrochemical experiments

Each cathode material was tested under strict anaerobic conditions, at 35 ºC, in a three-electrode/two-chamber system. All experiments were carried out under dark conditions to avoid phototrophic activity. Glass bottles were specifically designed, with a cathode chamber volume of approximately 300 mL. A 1 cm diameter, 15 cm long glass tube was inserted through the bottle top and served as the anode chamber, with a platinum wire as counter electrode (purity 99.95%, 0.50 mm diameter x 50 mm long, Advent Research Materials, Oxford, England). The chambers are separated by a cation exchange membrane (CEM) (Ultrex CM17000, Membranes International, NJ, USA). Two ports were placed in order to take samples from both the liquid phase and the headspace. A custom-made KCl saturated Ag/AgCl reference electrode was inserted into the bottle in proximity of the cathode. All potentials are reported here versus Standard Hydrogen Electrode (SHE). The BESs were operated in fed-batch mode. A multi-channel potentiostat (CH Instruments, Austin, TX, USA) was used for all experiments. During all experiments, the cathode was poised chronoamperometrically at -0.85 V. The total charge (Coulomb) consumed was calculated by integrating the area under the current versus time curve (i-t curve). A gas bag (Flexfoil plus, Air-Met Scientific Pty Ltd, QLD, Australia), specified for collection of CO_2, H_2 and CH_4, was connected to the reactors to measure gas composition and production rate and avoid pressure increase within the cathode chamber.
The cathode chamber was filled with 250 mL (acetic acid production rates and CO_2 consumption rates are calculated using this value) of a medium containing: 0.2 g L^{-1} NH_4CL, 0.04 g L^{-1} $MgCl_2.6H_2O$, 0.015 g L^{-1} $CaCl_2$, 6 g L^{-1} Na_2HPO_4, 3 g L^{-1} KH_2PO_4 and 1 mL L^{-1} of a trace element solution. This trace element solution contained 1.5 g L^{-1} $FeCl_3{\cdot}6H_20$, 0.15 g L^{-1}, H_3BO_3, 0.03 g L^{-1}, $CuSO_4{\cdot}5H_2O$, 0.18 g L^{-1} KI, 0.12 g L^{-1}, $MnCl_2{\cdot}4H_2O$, 0.06 g L^{-1}, $Na_2MoO_4{\cdot}2H_2O$, 0.12 g L^{-1}, $ZnSO_4{\cdot}7H_2O$, 0.15 g L^{-1}, $CoCl_2{\cdot}6H_2O$, 0.023 g L^{-1}, $NiCl_2{\cdot}6H_2O$, and 10 g L^{-1} EDTA.
Final concentration of 0.5 to 2 g L^{-1} $NaHCO_3$ was added periodically to the reactors as sole carbon source. To suppress methanogenic activity, 15mM 2-bromoethanesulfonic acid was initially added. The medium was prepared under anaerobic conditions (flushed with 100% N_2) and introduced into the cathode compartment inside an anaerobic chamber. During experiments, the catholyte medium pH was regularly adjusted to 7 by dosing 1M HCl as needed. The anolyte contained 44 mg L^{-1} Na_2HPO_4, and 25 mg L^{-1} KH_2PO_4.

Replicate electrodes:
Duplicate electrodes were tested for graphite plates, RVC, NanoWeb-RVC, EPD-3D 10ppi, and EPD-3D 60ppi. The two electrodes of each kind were immersed in the same electrochemical reactor and connected to different channels of a multipotentiostat (i.e. 2 RVC in reactor#1; 2 NanoWeb-RVC in reactor#2; 2 EPD-3D 10ppi in reactor#3; etc.). Hence, independent current values (and hence electron

consumptions) were obtained for each replicate. The values shown in figures 3A and 3B are the average of the two replicates.
Since two electrodes of each kind were immersed in the same reactor there is only one value for acetate production and CO_2 consumption for each kind of electrode, corresponding to the addition of the two electrodes. Thus, while this way of measuring does not strictly correspond to duplicate electrodes, small variabilities between electrodes are still averaged. It should be stressed that minimum variations were observed for the current values, hence re-enforcing our methodology.
The 2 EDP-3D 45ppi replicate electrodes were immersed individually in independent reactors. Thus, for EPD-3D independent replicate values were obtained for current, CO_2 consumption, and acetate production.

Analytical methods

Liquid samples (11.5 mL) were taken out of the cathode compartment through a rubber stopper using a 15 mL syringe equipped with a sterile needle, and were immediately filtered through a 0.22 µm filter.
Volatile fatty acids were measured using a gas chromatography (GC) apparatus (Agilent Technologies 7890A GC System) equipped with a flame ionisation detector (FID; 10 mL min^{-1} N_2; 250ºC) and a polar capillary column (DB-FFAP 15 m x 0.53 mm x 1.0 µm). High purity helium flowing with an initial flow of 12.5 mL min^{-1} was used as carrier gas. 0.9 mL sample was added to 0.1 mL of 10% formic acid solution and 0.5 µL of this mixture were injected in pulsed splitless at 220ºC.
Analytik Jena multi N/C 2100S Total Organic Carbon Analyser was used for the total inorganic carbon (TIC) analysis and followed the bicarbonate consumption. 250 µL samples were injected into a 2.6 M phosphoric acid solution and the resulting carbon dioxide was stripped of the solution and into the near infrared detector with a stream of oxygen.
5mL gas samples were taken from the reactor headspace using a gas tight syringe. Beforehand, the gas bag was disconnected from the reactor and the volume of gas produced between two sampling steps was assessed and a N_2-full gas bag was connected to the reactor. Methane, hydrogen and carbon dioxide gases were measured on a gas chromatography-Thermal Conductivity Detection (GC-TCD). The system was a Perkin Elmer auto system GC-TCD with a 2.44 m stainless steel column packed with Haysep (80/100 mesh). The GC was fitted with a GC Plus Data station, Model 1022 (Perkin Elmer, Waltham, MA, USA). High purity nitrogen (99.99%) was used as carrier gas at a flow rate of 24.3 mL/min and a pressure of 380 kPa. The injection port, oven and detector were operated at 75 ºC, 40 ºC and 100 ºC, respectively.
Optical density of non-filtered samples was assessed using a UV-visible spectrophotometer (Varian, Cary 50 Conc UV-Visible Spectrophotometer, California, USA) at 660 nm.

Calculations

Key performance indicators in table 1:

Values reported in table 1 correspond to the maximum performance indicators obtained in the mature reactors, i.e. after full development of the biofilms. The reported values are the performance indicators averaged during: the whole 140 day period for RVC; day 55 to 140 for graphite plates; from day 91 to 140 for NanoWeb- RVC; and from day 44 to 63 for EPD-3D.

Cumulative electron uptake:

The amount of coulomb taken up from the cathode between two time points t1 and t2 is calculated as the integral below, with I the current and t the time:

$$_{t1}^{t2}Coulomb = \int_{t1}^{t2} Idt$$

This is then converted to mol of electron (n_{e^-}) taken up between t1 and t2 as follow, with F the Faraday constant (96485 C $mol_{e^-}^{-1}$):

$$_{t1}^{t2}n_{e^-} = \frac{_{t1}^{t2}Coulomb}{F}$$

In the manuscript, mol of electron taken up was calculated between two sampling points, and added up over time to plot the cumulative electron uptake as represented in Figure 3.

Electron uptake rate into H_2 (as represented in Figure 7B):

The TOGA sensor was operated such that H_2 production rate was measured in mL min^{-1}. The measured flow rates of H_2 in mL min^{-1} were converted to mL of H_2 (V) and then to mol of H_2 (n_{H2}) using the ideal gas law as follow:

$$n_{H2} = \frac{PV}{RT}$$

With P and T the pressure and temperature, and R the ideal gas constant.

n_{H2} was then converted in mol of electron assimilated into H_2 ($n_{e^- into\ H2}$) as follow:

$$n_{e-into\ H2} = 2 \times n_{H2}$$

And further converted to current assimilated into H_2 using Faraday's law ($I_{into\ H2}$, in A):

$$I_{into\ H2} = \frac{n_{e-into\ H2} \times 96485}{(t_2 - t_1)}$$

With (t_2-t_1) in seconds.

Calculated acetate production rate during linear sweep voltammetry experiments, as represented in Figure 7A:

We experimentally proved during long-term chronoamperometry experiments that 100 ± 4% of the electrons were recovered into acetate + H_2, and that when CO_2 is fed only acetate is produced/detected and H_2 is not detected / does not escape the biofilm before it is consumed. Based on this experimental observation, and that linear sweep voltammetry experiment at 1 mV/s scan rate was too short to measure any quantifiable acetate concentration change in the catholyte (due to large catholyte volume/electrode volume ratio), we estimated acetate production rate during LSV from the difference of total electron uptake rate and electron uptake rate into H_2, as follow:

Between each data point, n_{e^-} and $n_{e^- into\ H2}$ were determined from the potentiostat and TOGA data as explained above.

$$n_{e-into\ acetate} = n_{e^-} - n_{e-into\ H2}$$

$$n_{acetate} = \frac{n_{e-into\ acetate}}{8}$$

With $n_{acetate}$ the amount of acetate produced between two time points (in mol), and 8 the number of electron necessary to reduce 2 molecules of CO_2 into one molecule of acetate.

$$Acetate\ production\ rate\ (g\ m^{-2}day^{-1}) = \frac{n_{acetate} \times M_{acetate}}{(t_2 - t_1) \times PSA}$$

With PSA the projected surface area of the cathode in m^2.

Microbial Community Analysis

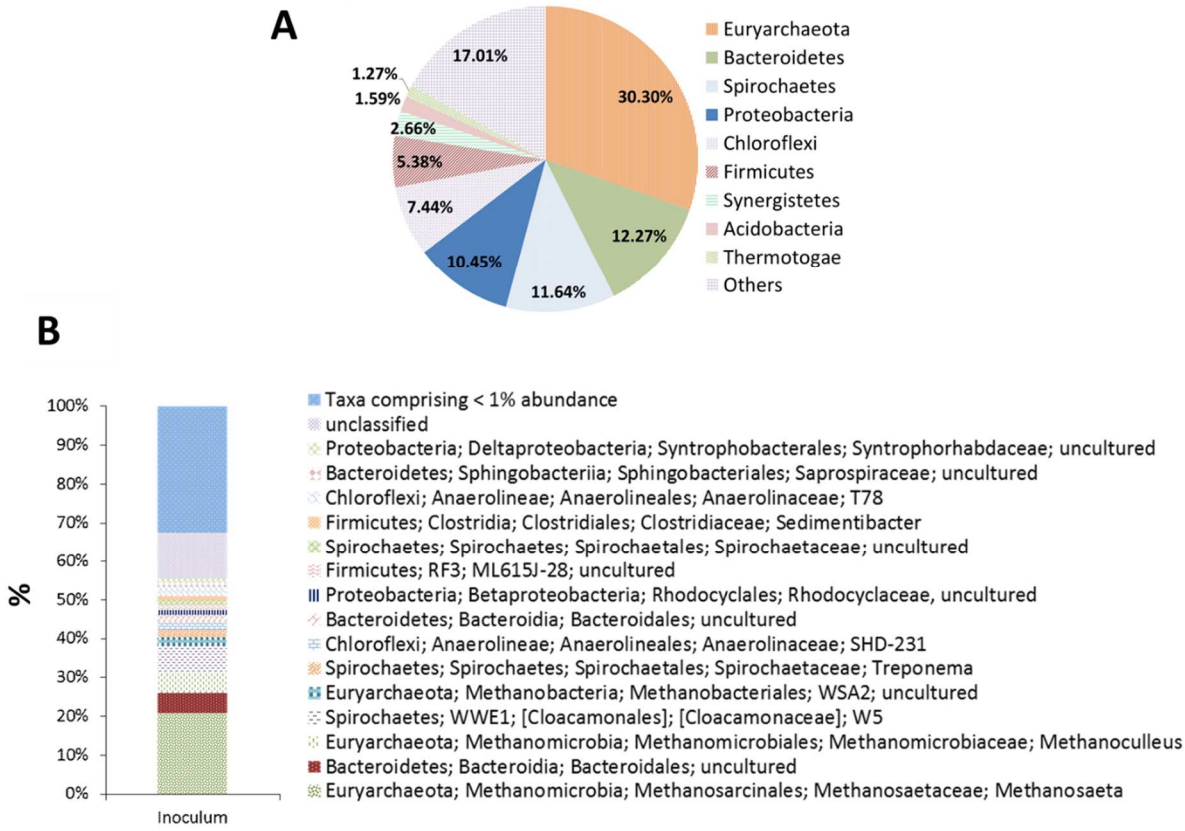

Figure S2. A) Phylum distribution of the original inoculum - Fractions shown as "Others" consist of phylogenetic groups with <1% abundance each and/or no blast hit. B) Percent abundance of 16S rRNA from the original inoculum. Reproduced from [1].

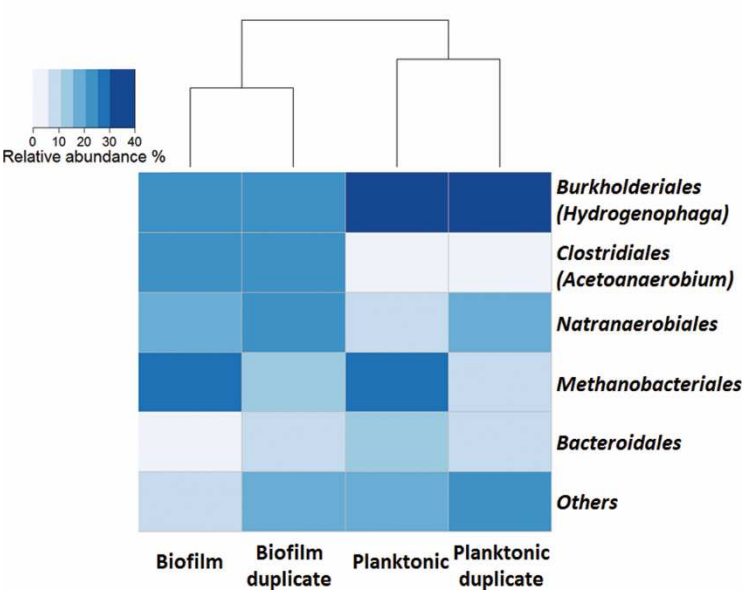

Figure S3. Heatmap of microbial community in biofilm and planktonic cells from two replicate reactors based on order-level summary from pyrosequencing analysis. Genus information is also provided in brackets if it dominates in the corresponding order. Other orders that contains OTUs with less than 1% relative abundance are summarized and presented as "Others". Reproduced from [1].

Table S1. Literature used to produce Figure 1 in the core of the manuscript, with the reported current density and organics production rates normalized to projected surface area of the cathode. We used current density and organics productivity recorded during the same period of time when possible; otherwise we used the maximum values of productivity and current density, which explains that few data points exceed the 100% coulombic efficiency. Some studies are not reported in this table because the current density or production rates normalized to projected surface area were not given or could not be calculated from the information provided.

Cathode material	Current density ($A\ m^{-2}$)	Production rate ($g\ m^{-2}_{psa}\ day^{-1}$)	Reference
Graphite rods	-0.21	1.30	Nevin et al. 2010 [2]
Graphite rods	-0.03	0.14	Nevin et al. 2011 [3]
Carbon cloth (CC)	-0.07	0.35	Zhang et al. 2013 [4]
CC-chitosan	-0.48	2.70	
CC-cyanuric acid	-0.45	2.42	
CC-3-Aminopropyltriethoxysilane	-0.21	1.12	
CC-Polyaniline	-0.19	1.06	
CC-Melanine	-0.07	0.37	
CC-Ammonia	-0.06	0.33	
CC-Au	-0.39	2.14	
CC-Pd	-0.32	1.66	
CC-Ni	-0.30	1.60	
CNT-cotton	-0.22	1.20	
CNT-polyester	-0.21	1.13	
Graphite plate	0.49	2.94	Gong et al. 2013 [5]
Carbon felt	-3.37	0	Jiang et al. 2013 [6]
	-9.29	16.39	
Carbon felt	-3.44	11.63	Su et al. 2013 [7]
Ni-nanowire-network-coated graphite stick	-0.69	3.33	
Ni-nanoparticle-coated graphite stick	-0.15	0.90	
Carbon fiber rod	-0.03	0.05	Zaybak et al. 2013 [8]
Graphite rod	-1.76	5.75	Jourdin et al. 2014 [9]
Unmodified RVC	-3.70	0.00	
NanoWeb-RVC	-37.00	191.75	
Graphite rods	-0.92	8.56	LaBelle et al. 2014 [10]
Graphite felt	-2.80	10.10	Xafenias et al. 2014 [11]
Carbon cloth	-20	10.57	Ganigue et al. 2015 [12]
Graphite plate	-0.35	0.56	Modestra et al. 2015 [13]
Graphite stick	-0.71	4.07	Giddings et al. 2015 [14]
	-1.70	9.68	

Circular graphite disk	-0.17	1.65	
	-0.48	2.12	
Carbon-felt-Stainless steel assembly	-5.00	39.83	Bajracharya et al. 2015 [15]
	-1.00	18.88	
Carbon felt	-5	19.00	Patil et al. 2015 [16]
VITO-CoRE-PL (VC-IS, plastic inert support)	-0.12	9.49	Mohanakrishna et al. 2015 [17]
Graphite rod	-0.05	3.45	
Carbon felt with a stainless steel frame current collector	-5.00	20.40	Gildemyn et al. 2015 [18]
Stainless steel plate	-1.50	4.96	Blanchet et al. 2015 [19]
graphite stick	-0.32	1.97	Tremblay et al. 2015 [20]
	-2.16	12.78	
EPD-3D 45 ppi	-102.00	685.00	Jourdin et al. 2015 and Jourdin et al. 2016a [1, 21]
EPD-3D 45 ppi	-102.00	685.00	Jourdin et al. 2016b [22]
EPD-3D 10 ppi	-35.00	247.00	
EPD-3D 60 ppi	-93.00	620.00	
Graphite felt + SS plate current collector	-2.26	8.21	Molenaar et al. 2016 [23]
Graphite stick	-0.33	1.89	Ammam et al. 2016 [24]
	-1.4	8.33	
Unmodified carbon felt	-0.4	2.01	Aryal et al. 2016 [25]
Carbon felt coated with 3D graphene	-2.45	13.65	
VITO-Core® GDE	-20	36.6	Bajracharya et al. 2016 [26]
Carbon cloth	-0.191	1.8172	Chen et al. 2016 [27]
rGO-TEPA-nanoparticles modified-carbon cloth	-0.686	6.62865	
Carbon cloth	-0.42	3.94415	
rGO-TEPA-nanoparticles modified-carbon cloth	-2.358	21.7238	
Graphite stick	-0.52	0.1357	Deutzmann et al. 2016 [28]
	-1.05	0.4366	
Graphite stick	-0.45	2.02	Aryal et al. 2017 [29]
	-0.783	3.60	
	-0.191	0.76	
	-0.572	2.60	
	-0.703	2.68	
	-0.026	0	
Graphite stick with 2 graphite felts wrapped around	-20	16.6	Bajracharya et al. 2017a [30]

Graphite stick with 2 graphite felts wrapped around	-15	22.2	Bajracharya et al. 2017b [31]
Graphite felt	-0.83	3.827625	Cui et al. 2017 [32]
3D Iron oxide graphitized carbon felt	-1.88	18.29	
Graphite felt	-5	9.5	Gyldemyn et al. 2017 [33]
	-5	19.2	
	-5	10.7	
Unmodified reticulated vitreous carbon	-83.3	196.8	Labelle et al. 2017 [34]
Graphite felt	-11	60	Molenaar et al. 2017 [35]
Graphite plate	-0.37	1.06613	Xiang et al. 2017 [36]
Graphite felt	-5	18.8	Arends et al. 2017 [37]
Plain graphite plate loaded with carbon powder	-16.2	49.7	Srikanth et al. 2017 [38]
Graphite felt	-120	577	Jourdin et al. 2018 [39]
Graphite granules	-9	26.3	Vassilev et al. 2018 [40]
VITO-Core® GDE	-10	19.2	Srikanth et al. 2018 [41]
Nickel foam	-7.2	22.8	Song et al. 2018 [42]
Graphene–nickel foam	-10.2	41.9	
Graphite felt	-31.1	84.03	Das et al. 2018 [43]
Granular activated carbon particles + Carbon felt	-4.08	7.84	Dong et al. 2018 [44]
Graphite stick placed between two graphite felts	-25	6.9	Rojas et al. 2018 [45]
Ti mesh with coated Pt/C	-1.63	9.78	Li et al. 2018 [46]
		1.96	
	-1.63	11.74	
Graphite plates	-0.0462	0.42	Chen et al. 2018 [47]
Carbon felt	-0.74	0.12	Mateos et al. 2018 [48]
Graphite felt	-126	400.7	Jourdin et al. 2019 [49]
Carbon felt	-3.7	375.438	Anwer et al. 2019 [50]
MnO2 coated carbon felt	-1.7	225.564	
Zn foil pressed onto carbon felt	-30	136	Jiang et al. 2019 [51]
	-50	300	
5 cm × 5 cm carbon felt	-4	28	Song et al. 2019 [52]
Titanium carbide (Ti3C2TX MXene) coated on carbon felt	-0.15	17.08	Tahir et al. 2020 [53]
Carbon felt	-0.05	11.43	

Graphite plates	-0.317	1.58	Tremblay et al. 2019 [54]
Molybdenum carbide (Mo2C)-modified carbon felt	-5.2	21.28	Tian et al. 2019 [55]
Carbon felt	-2.4	10.45	
Graphite felt	-0.317	0.444	Hou et al. 2019 [56]
Reduced graphene oxide-coated copper foam	-21.6	100.16	Aryal et al. 2019 [57]
Copper foam	-7.1	4.70	
Reduced graphene oxide foam	-2.6	13.22	
reduced oxide graphene foam electroplated with copper	-4.3	2.30	
Cylindrical graphite felt	-3	2.79	Mateos et al. 2019 [58]
NiMo	-10	1.125	Kracke et al. 2019 [59]

References (different numbers than main text references)

1. Jourdin, L., et al., *High acetic acid production rate obtained by microbial electrosynthesis from carbon dioxide.* Environmental Science & Technology, 2015. **49**(22): p. 13566-13574.
2. Nevin, K.P., et al., *Microbial electrosynthesis: Feeding microbes electricity to convert carbon dioxide and water to multicarbon extracellular organic compounds.* mBio, 2010. **1**(2): p. 1-4.
3. Nevin, K.P., et al., *Electrosynthesis of organic compounds from carbon dioxide is catalyzed by a diversity of acetogenic microorganisms.* Applied and Environmental Microbiology, 2011. **77**(9): p. 2882-2886.
4. Zhang, T., et al., *Improved cathode materials for microbial electrosynthesis.* Energy & Environmental Science, 2013. **6**(1): p. 217-224.
5. Gong, Y., et al., *Sulfide-Driven Microbial Electrosynthesis.* Environmental Science & Technology, 2013. **47**(1): p. 568-573.
6. Jiang, Y., et al., *Bioelectrochemical systems for simultaneously production of methane and acetate from carbon dioxide at relatively high rate.* International Journal of Hydrogen Energy, 2013(0).
7. Min, S., Y. Jiang, and D. Li, *Production of acetate from carbon dioxide in bioelectrochemical systems based on autotrophic mixed culture.* Journal of Microbiology and Biotechnology, 2013. **23**(8): p. 1140-1146.
8. Zaybak, Z., et al., *Enhanced start-up of anaerobic facultatively autotrophic biocathodes in bioelectrochemical systems.* Journal of Biotechnology, 2013(0).
9. Jourdin, L., et al., *A novel carbon nanotube modified scaffold as an efficient biocathode material for improved microbial electrosynthesis.* Journal of Materials Chemistry A, 2014. **2**(32): p. 13093-13102.
10. LaBelle, E.V., et al., *Influence of acidic pH on hydrogen and acetate production by an electrosynthetic microbiome.* PLoS ONE, 2014. **9**(10): p. e109935.
11. Xafenias, N. and V. Mapelli, *Performance and bacterial enrichment of bioelectrochemical systems during methane and acetate production.* International Journal of Hydrogen Energy, 2014. **39**: p. 21864-21875.
12. Ganigue, R., et al., *Microbial electrosynthesis of butyrate from carbon dioxide.* Chemical Communications, 2015. **51**(15): p. 3235-3238.

13. Modestra, J.A. and S.V. Mohan, *Microbial electrosynthesis of carboxylic acids through CO2 reduction with selectively enriched biocatalyst: Microbial dynamics.* Journal of CO2 Utilization, 2017. **20**: p. 190-199.
14. Giddings, C.G.S., et al., *Simplifying Microbial Electrosynthesis Reactor Design.* Frontiers in Microbiology, 2015. **6**: p. 1-6.
15. Bajracharya, S., et al., *Carbon dioxide reduction by mixed and pure cultures in microbial electrosynthesis using an assembly of graphite felt and stainless steel as a cathode.* Bioresource Technology, 2015. **195**: p. 14-24.
16. Patil, S.A., et al., *Selective Enrichment Establishes a Stable Performing Community for Microbial Electrosynthesis of Acetate from CO2.* Environmental Science & Technology, 2015. **49**(14): p. 8833-8843.
17. Mohanakrishna, G., et al., *An enriched electroactive homoacetogenic biocathode for the microbial electrosynthesis of acetate through carbon dioxide reduction.* Faraday Discussions, 2015. **183**: p. 445-462.
18. Gildemyn, S., et al., *Integrated Production, Extraction, and Concentration of Acetic Acid from CO2 through Microbial Electrosynthesis.* Environmental Science & Technology Letters, 2015. **2**(11): p. 325–328.
19. Blanchet, E., et al., *Importance of the hydrogen route in up-scaling electrosynthesis for microbial CO 2 reduction.* Energy & Environmental Science, 2015. **8**(12): p. 3731-3744.
20. Tremblay, P.-L., et al., *Adaptation of the autotrophic acetogen Sporomusa ovata to methanol accelerates the conversion of CO2 to organic products.* 2015. **5**: p. 16168.
21. Jourdin, L., et al., *Biologically-induced hydrogen production drives high rate/high efficiency microbial electrosynthesis of acetate from carbon dioxide.* ChemElectroChem, 2016. **3**(4): p. 581-591.
22. Jourdin, L., et al., *Bringing high-rate, CO2-based microbial electrosynthesis closer to practical implementation through improved design and operating conditions.* Environmental Science & Technology, 2016. **50**(4): p. 1982-1989.
23. Molenaar, S.D., et al., *Microbial Rechargeable Battery: Energy Storage and Recovery through Acetate.* Environmental Science & Technology Letters, 2016. **3**(4): p. 144-149.
24. Ammam, F., et al., *Effect of tungstate on acetate and ethanol production by the electrosynthetic bacterium Sporomusa ovata.* Biotechnology for Biofuels, 2016. **9**(1): p. 163.
25. Aryal, N., et al., *Enhanced microbial electrosynthesis with three-dimensional graphene functionalized cathodes fabricated via solvothermal synthesis.* Electrochimica Acta, 2016. **217**: p. 117-122.
26. Bajracharya, S., et al., *Application of gas diffusion biocathode in microbial electrosynthesis from carbon dioxide.* Environmental Science and Pollution Research, 2016. **23**(22): p. 22292-22308.
27. Chen, L., et al., *Electrosynthesis of acetate from CO 2 by a highly structured biofilm assembled with reduced graphene oxide–tetraethylene pentamine.* Journal of Materials Chemistry A, 2016. **4**(21): p. 8395-8401.
28. Deutzmann, J.S. and A.M. Spormann, *Enhanced microbial electrosynthesis by using defined co-cultures.* The ISME Journal, 2016.
29. Aryal, N., et al., *Performance of different Sporomusa species for the microbial electrosynthesis of acetate from carbon dioxide.* Bioresource Technology, 2017. **233**: p. 184-190.
30. Bajracharya, S., et al., *In situ acetate separation in microbial electrosynthesis from CO 2 using ion-exchange resin.* Electrochimica Acta, 2017.
31. Bajracharya, S., et al., *Long-term operation of microbial electrosynthesis cell reducing CO2 to multi-carbon chemicals with a mixed culture avoiding methanogenesis.* Bioelectrochemistry, 2017. **113**: p. 26-34.
32. Cui, M., et al., *Three-dimensional Hierarchical Metal oxide-Carbon Electrode Material for High Efficient Microbial Electrosynthesis.* Sustainable Energy & Fuels, 2017. **1**: p. 1171-1176.

33. Gildemyn, S., et al., *The type of ion selective membrane determines stability and production levels of microbial electrosynthesis.* Bioresource Technology, 2017. 224: p. 358-364.
34. LaBelle, E.V. and H.D. May, *Energy Efficiency and Productivity Enhancement of Microbial Electrosynthesis of Acetate.* Frontiers in Microbiology, 2017. 8: p. 756.
35. Molenaar, S., et al., *Competition between Methanogens and Acetogens in Biocathodes: A Comparison between Potentiostatic and Galvanostatic Control.* International Journal of Molecular Sciences, 2017. 18(1): p. 204.
36. Xiang, Y., et al., *High-efficient acetate production from carbon dioxide using a bioanode microbial electrosynthesis system with bipolar membrane.* Bioresource Technology, 2017. 233: p. 227-235.
37. Arends, J.B.A., et al., *Continuous long-term electricity-driven bioproduction of carboxylates and isopropanol from CO2 with a mixed microbial community.* Journal of CO2 Utilization, 2017. 20: p. 141-149.
38. Srikanth, S., et al., *Long-term operation of electro-biocatalytic reactor for carbon dioxide transformation into organic molecules.* Bioresource Technology, 2017. 265: p. 66-74.
39. Jourdin, L., et al., *Critical biofilm growth throughout unmodified carbon felts allows continuous bioelectrochemical chain elongation from CO2 up to caproate at high current density.* Frontiers in Energy Research, 2018. 6: p. 7.
40. Vassilev, I., et al., *Microbial Electrosynthesis of Isobutyric, Butyric, Caproic Acids, and Corresponding Alcohols from Carbon Dioxide.* ACS Sustainable Chemistry & Engineering, 2018. 6(7): p. 8485-8493.
41. Srikanth, S., et al., *Electro-biocatalytic conversion of carbon dioxide to alcohols using gas diffusion electrode.* Bioresource Technology, 2018. 265: p. 45-51.
42. Song, T.-s., et al., *High efficiency microbial electrosynthesis of acetate from carbon dioxide using a novel graphene–nickel foam as cathode.* Journal of Chemical Technology & Biotechnology, 2018. 93(2): p. 457-466.
43. Das, S., P. Chatterjee, and M.M. Ghangrekar, *Increasing methane content in biogas and simultaneous value added product recovery using microbial electrosynthesis.* Water Science and Technology, 2018. 77(5): p. 1293-1302.
44. Dong, Z., et al., *Fluidized granular activated carbon electrode for efficient microbial electrosynthesis of acetate from carbon dioxide.* Bioresource Technology, 2018. 269: p. 203-209.
45. Rojas, M.d.P.A., et al., *Microbial electrosynthesis (MES) from CO2 is resilient to fluctuations in renewable energy supply.* Energy Conversion and Management, 2018. 177: p. 272-279.
46. Li, X., I. Angelidaki, and Y. Zhang, *Salinity-gradient energy driven microbial electrosynthesis of value-added chemicals from CO 2 reduction.* Water research, 2018.
47. Chen, S., et al., *Enhanced electrosynthesis performance of Moorella thermoautotrophica by improving cell permeability.* Bioelectrochemistry, 2018. 121: p. 151-159.
48. Mateos, R., et al., *Impact of the start-up process on the microbial communities in biocathodes for electrosynthesis.* Bioelectrochemistry, 2018. 121: p. 27-37.
49. Jourdin, L., et al., *Enhanced selectivity to butyrate and caproate above acetate in continuous bioelectrochemical chain elongation from CO2: Steering with CO2 loading rate and hydraulic retention time.* Bioresource Technology Reports, 2019. 7: p. 100284.
50. Anwer, A.H., et al., *Development of novel MnO2 coated carbon felt cathode for microbial electroreduction of CO2 to biofuels.* Journal of Environmental Management, 2019. 249: p. 109376.
51. Jiang, Y., et al., *Zinc: A promising material for electrocatalyst-assisted microbial electrosynthesis of carboxylic acids from carbon dioxide.* Water Research, 2019. 159: p. 87-94.
52. Song, T.-s., et al., *Experimental evaluation of the influential factors of acetate production driven by a DC power system via CO2 reduction through microbial electrosynthesis.* Bioresources and Bioprocessing, 2019. 6(1): p. 29.

53. Tahir, K., et al., *A novel MXene-coated biocathode for enhanced microbial electrosynthesis performance.* Chemical Engineering Journal, 2020. **381**: p. 122687.
54. Tremblay, P.-L., N. Faraghiparapari, and T. Zhang, *Accelerated H2 Evolution during Microbial Electrosynthesis with Sporomusa ovata.* Catalysts, 2019. **9**(2): p. 166.
55. Tian, S., et al., *Mo2C-induced hydrogen production enhances microbial electrosynthesis of acetate from CO2 reduction.* Biotechnology for Biofuels, 2019. **12**(1): p. 71.
56. Hou, X., et al., *Electrosynthesis of acetate from inorganic carbon (HCO3−) with simultaneous hydrogen production and Cd(II) removal in multifunctional microbial electrosynthesis systems (MES).* Journal of Hazardous Materials, 2019. **371**: p. 463-473.
57. Aryal, N., et al., *Increased carbon dioxide reduction to acetate in a microbial electrosynthesis reactor with a reduced graphene oxide-coated copper foam composite cathode.* Bioelectrochemistry, 2019. **128**: p. 83-93.
58. Mateos, R., et al., *Enhanced CO2 Conversion to Acetate through Microbial Electrosynthesis (MES) by Continuous Headspace Gas Recirculation.* Energies, 2019. **12**(17): p. 3297.
59. Kracke, F., et al., *Robust and biocompatible catalysts for efficient hydrogen-driven microbial electrosynthesis.* Communications Chemistry, 2019. **2**(1): p. 45.